Neurospine 2018;15(4):306-322.
https://doi.org/10.14245/ns.1836206.103

Neurospine
pISSN 2586-6583 eISSN 2586-6591

Review Article

Review of Photoacoustic Imaging for Imaging-Guided Spinal Surgery

Seung Hee Han[1,2]

[1]Division of Biophotonics, Princess Margaret Hospital, University Health Network, Toronto, ON, Canada
[2]Department of Medical Biophysics, University of Toronto, Toronto, ON, Canada

Corresponding Author
Seung Hee Han
https://orcid.org/0000-0003-4900-3360

Division of Biophotonics, Princess Margaret Hospital, University Health Network, Toronto, ON M5G 2C4, Canada
E-mail: shan@uhnres.utoronto.ca
Tel: +1-4166682790

Received: September 7, 2018
Revised: November 1, 2018
Accepted: November 10, 2018

This review introduces the current technique of photoacoustic imaging as it is applied in imaging-guided surgery (IGS), which provides the surgeon with image visualization and analysis capabilities during surgery. Numerous imaging techniques have been developed to help surgeons perform complex operations more safely and quickly. Although surgeons typically use these kinds of images to visualize targets hidden by bone and other tissues, it is nonetheless more difficult to perform surgery with static reference images (e.g., computed tomography scans and magnetic resonance images) of internal structures. Photoacoustic imaging could enable real-time visualization of regions of interest during surgery. Several researchers have shown that photoacoustic imaging has potential for the noninvasive diagnosis of various types of tissues, including bone. Previous studies of the surgical application of photoacoustic imaging have focused on cancer surgery, but photoacoustic imaging has also recently attracted interest for spinal surgery, because it could be useful for avoiding pedicle breaches and for choosing an appropriate starting point before drilling or pedicle probe insertion. This review describes the current instruments and clinical applications of photoacoustic imaging. Its primary objective is to provide a comprehensive overview of photoacoustic IGS in spinal surgery.

Keywords: Photoacoustic imaging, Imaging-guided surgery, Minimally surgery, Spinal surgery, Robot surgery

INTRODUCTION

Imaging-guided surgery (IGS) is classified within the broader category of computer-assisted surgery.[1] Through IGS, the spine surgeon is able to see the procedure as it is performed in real time. The technique of IGS has been developing since the early 1990s, and it is now used on a daily basis in the field of spinal surgery, including cancer surgery. Numerous imaging techniques have been developed to help surgeons perform complex operations more safely and quickly; however, it is more difficult to perform surgery with static reference images (e.g., computed tomography scans and magnetic resonance images) of internal structures. Photoacoustic imaging could enable the real-time visualization of regions of interest during surgery.[2] The photoacoustic imaging technique detects optical contrasts at the spatial resolution of ultrasound using a short-pulse laser as the light source and a conventional ultrasound transducer as the imaging sensor. Furthermore, it is nonionizing and noninvasive; as such, it is the fastest-growing new method of biomedical imaging, with clinical applications under further development. The ultimate goal of this article is to review the current status of photoacoustic imaging technology and its applicability to IGS in the field of spinal surgery and cancer.

HISTORY OF PHOTOACOUSTIC IMAGING

Photoacoustic imaging, also known as optoacoustic imaging, is a truly fused multi-imaging modality. It has emerged over the last decade, and is based on the use of laser-generated ultrasound. Fig. 1 shows the history of photoacoustic imaging technology since 1980. The photoacoustic effect was first observed in 1880 by Alexander Graham Bell, the scientist credited with inventing the first practical telephone. Bell is considered to have discovered the photoacoustic effect by observing that sound was gen-

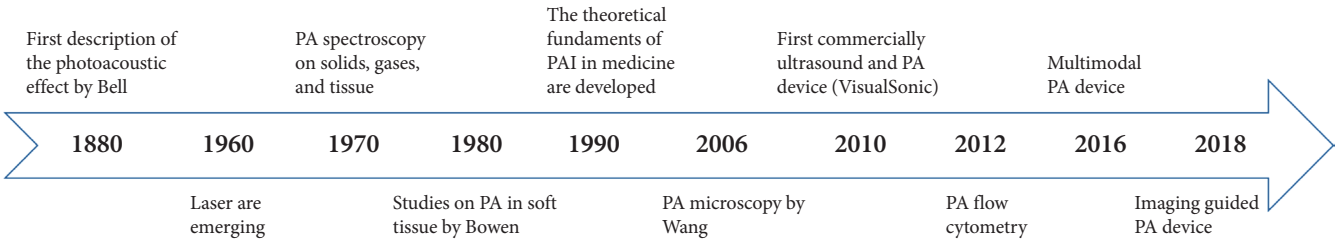

Fig. 1. The history of photoacoustic imaging. Several decades passed from Bell's first description of the photoacoustic effect to the development of clinical applications. PA, photoacoustic; PAI, photoacoustic imaging.

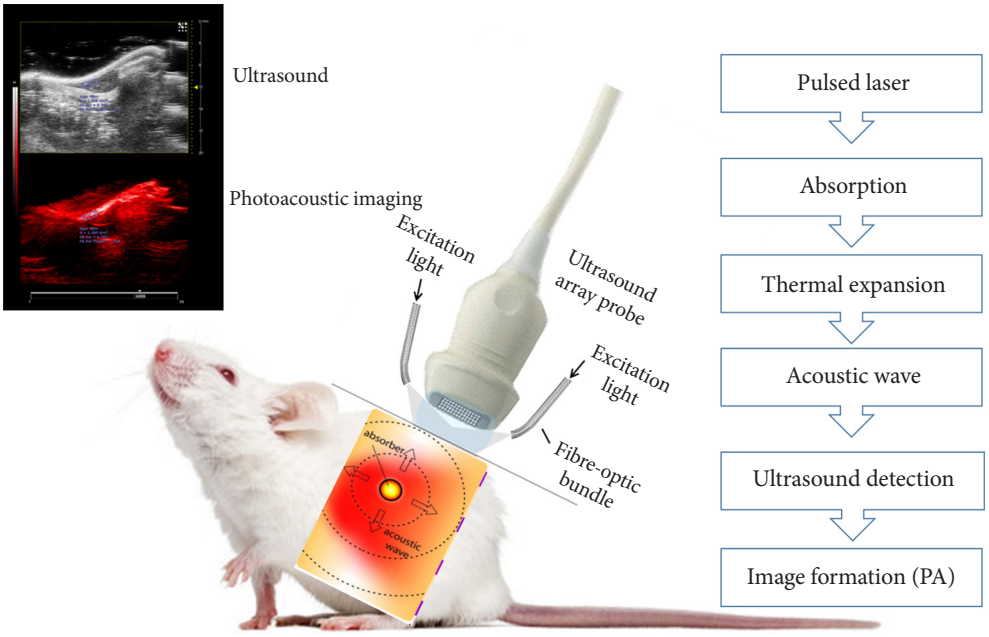

Fig. 2. The basic principle of photoacoustic imaging. When a tissue is exposed to pulsed near-infrared laser light, the constituents of the tissue (e.g., water, lipids, collagen, hemoglobin, etc.) absorb light and undergo thermoelastic expansion, thereby causing ultrasound signals to emanate (the photoacoustic effect). Therefore, these laser-induced ultrasound signals (photoacoustic signals) can be detected using an ultrasound transducer, making photoacoustic (or optoacoustic) imaging possible. Each of these biological absorbers can be targeted by irradiating tissue at the corresponding dominant absorption wavelength. As such, using a tunable laser at the relevant wavelengths of interest enables the acquisition of multiple photoacoustic images that can be spectrally resolved for tissue composition to be assessed based on endogenous contrast. PA, photoacoustic.

erated by the absorption of modulated sunlight.[3] In the 1990s, photoacoustic imaging began to be more seriously researched for medical applications due to advances in both laser light sources and acoustic detection equipment.[4]

PRINCIPLES OF PHOTOACOUSTIC IMAGING

In the photoacoustic effect, ultrasound waves are generated by a light-absorbing material following the absorption of modulated light, usually pulsed laser light on a nanosecond timescale. The absorbed light energy causes localized heating, which in turn produces a temperature rise, well below the amount that would produce physical damage or a phase change inside the object. This temperature increment gives rise to an initial pressure increase due to rapid thermal expansion. The pressure increase is followed by relaxation, generating broadband low-amplitude ultrasound waves. These ultrasound waves, better known as photoacoustic waves, are emitted from the object and can be captured by ultrasound transducers in different configurations depending upon the mode of imaging to produce a sequence of A-line signals.[5] An A-line signal is simply the display of the time-

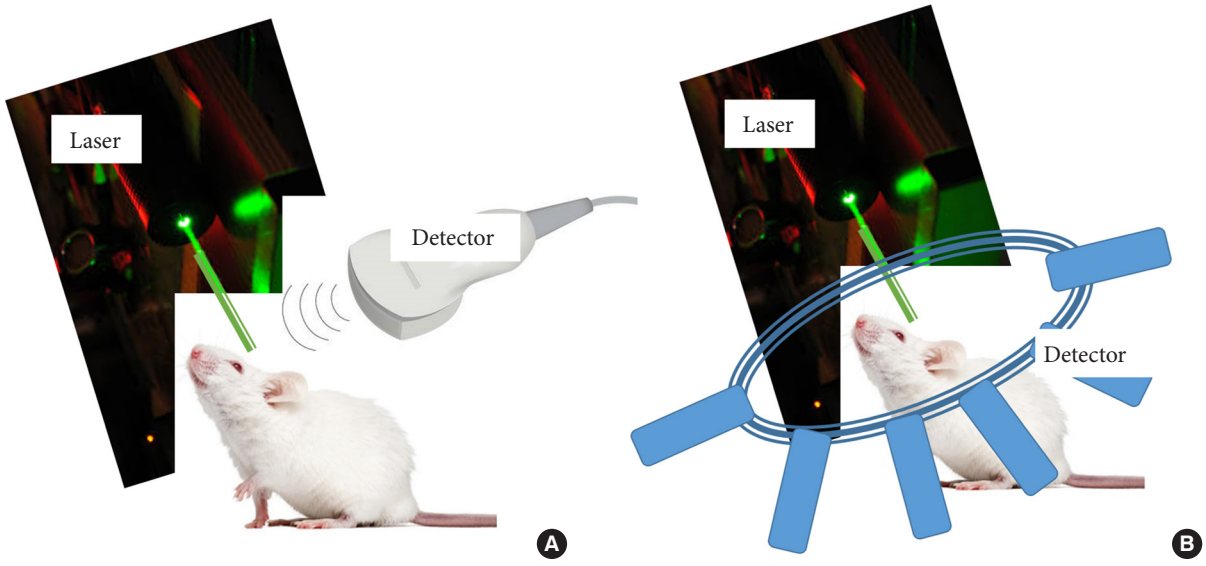

Fig. 3. Photoacoustic imaging configurations. The detectors and the laser source may be on the same side or at an angle to each other. (A) Photoacoustic imaging performed using a conventional ultrasound transducer, in which only part of the spherical wave front originating from the target is registered by the transducer. (B) Photoacoustic tomography showing X-ray computed tomography–like reconstruction, in which a single detector can be rotated around the target or an array of multiple stationary detector elements can be deployed around the target. The signal arriving at each detector is filtered, back-projected along circular arcs in the spatial domain, and all the back-projections are then added together to obtain the final photoacoustic image, which represents the spatial distribution of optical absorption within the target.

dependent response of the transducer generated by the ultrasound wave.[6] A-line signals are suitably processed and combined to produce 2-dimensional photoacoustic images of the materials. Fig. 2 shows the basic principles of photoacoustic imaging.

Photoacoustic imaging can be divided into 2 geometries, as shown in Fig. 3. For a handheld device, a linear transducer is used, which can only measure the ultrasound signal from a limited point of view, resulting in the limited view problem (Fig. 3A). Fig. 3B shows a more advantageous geometry, in which the transducers surround the tissue and a 360° scan is used to measure the signal.[7]

In photoacoustic imaging, both the resolution and the penetration depth correlate with the ultrasound frequency. Therefore, a higher ultrasound frequency of the photoacoustic signal results in better spatial resolution because the relative value decreases. The maximum penetration depth simultaneously decreases as well, because higher ultrasonic frequencies are more attenuated than lower frequencies. Thus, there is a trade-off between resolution and penetration depth. It should be kept in mind that this is only valid within the tissue area in which sufficient optical power is obtained for generating the optical sound waves. Its size may vary depending on the wavelength of radiation used. Near-infrared light can usually penetrate the tissue well, and the following relationship holds[4]:

$$\text{Relative Spatial Resolution} = \frac{\textit{Penetration Depth}}{\textit{Resolution}}$$

This definition is characteristic of high-resolution imaging modalities, which means that photoacoustic imaging can be considered such a modality. A microscopy system utilizing photoacoustic imaging was found to achieve a relative spatial resolution of roughly 200. Table 1 shows a comparison of the imaging technologies discussed above and summarizes their function.

INSTRUMENTS FOR PHOTOACOUSTIC IMAGING

Photoacoustic imaging systems typically include a pulsed near-infrared laser (532- to 1,100-nm wavelengths, 1- to 100-ns pulse width, and 10- to 50-Hz pulse repetition rate), an ultrasound transducer, and a data acquisition and display unit (Fig. 4). Photoacoustic imaging instruments can be categorized as preclinical and clinical imaging systems. Preclinical imaging systems typically use a small animal placement platform (with a selective heating pad to keep the animal warm during the procedure and respiratory gating to compensate for heart rate monitoring

https://doi.org/10.14245/ns.1836206.103

Table 1. Comparison of the performance of different imaging techniques

Variable	Ultrasound	Photoacoustic imaging	Fluorescence imaging	MRI	PET
Type of energy measured	High-frequency sound waves	High-frequency sound waves	Visible or near-infrared light	Radio waves	High energy gamma rays
Spatial resolution	50–500 μm	50–500 μm	2–10 mm (depth dependent)	20–100 μm	1–2 mm
Time resolution	Seconds to minutes	Seconds to minutes	Seconds	Minutes to hours	Minutes
Sensitivity	Not well characterized	pM	nM	μM–mM	pM
Depth	<5 cm	<5 cm	<5 mm	No limit	No limit
Type of contrast agents	Microbubble	Nanoparticle/microbubble	Small molecules nanoparticle	Small molecules nanoparticle	Small molecules nanoparticle
Cost	Low	Low	Medium	High	High

MRI, magnetic resonance imaging; PET, positron emission tomography.

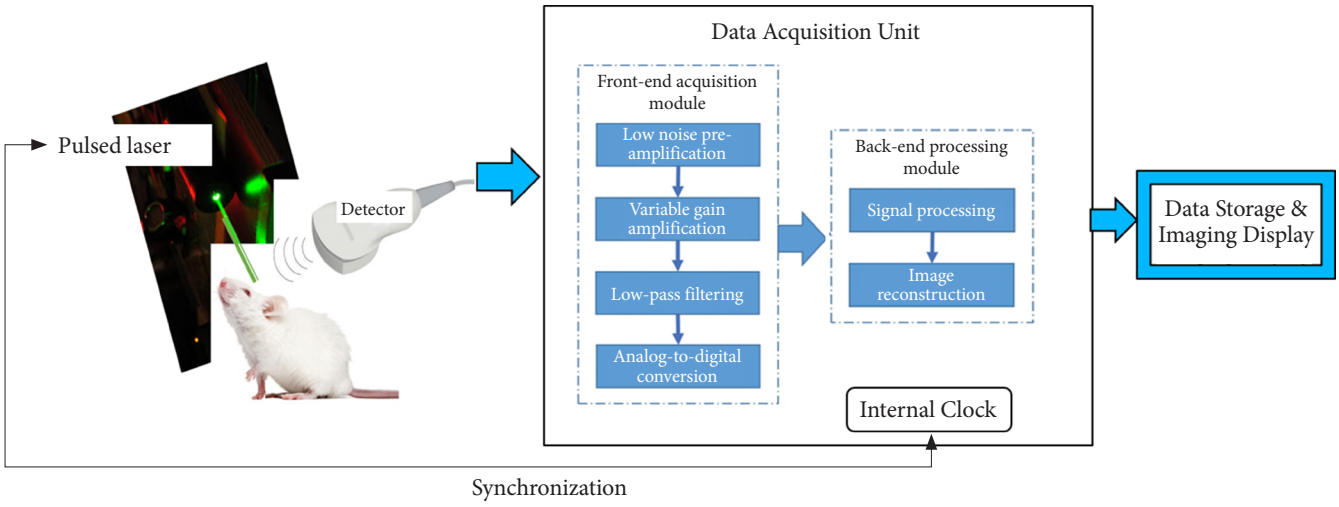

Fig. 4. Schematic of photoacoustic imaging instrumentation. When a tissue is exposed to pulsed near-infrared laser light, the transient pressure readings produced from tissue chromophores are collected by an ultrasound transducer scanned over the surface. An internal clock synchronizes the transducer acquisition time to laser firing. The transient pressure gradients are converted by the transducer to time-dependent voltage signals (photoacoustic signals) and are fed into a front-end acquisition module where the signals are channeled through a low-noise preamplifier (20–30 dB), followed by a variable gain amplifier (20–50 dB) to achieve a cumulative gain (40–80 dB). The amplified signals are filtered for high-frequency noise components and digitized using analog-to-digital converters. These digitized signals are further handled by a back-end processing module, which performs a multitude of signal processing and image reconstruction tasks, after which the images are appropriately stored and displayed.

and motion artifacts) and high-frequency transducers for high-resolution imaging. Fig. 5 shows 2 commercially available preclinical photoacoustic imaging system used currently.

VisualSonics first developed the Vevo LAZR-X (Fujifilm VisualSonics, Toronto, Canada; technology licensed from Seno Medical Instruments, San Antonio, TX, USA) photoacoustic platform for small-animal preclinical imaging, based on an ultrasound imaging system. Endra Life Sciences also manufactured the Nexus 128 (Ann Arbor, MI, USA; technology licensed from OptoSonics, Oriental, NC, USA) platform for small-animal photoacoustic imaging of cancers for preclinical use. Clinical photoacoustic imaging systems are a logical extension of preclinical imaging systems and use transducers with clinically relevant frequencies (1–10 MHz). Clinical photoacoustic imaging systems are often region-specific because different laser-detector configurations are preferred for different applications (e.g., tomography is suitable for the breast; low-frequency handheld transducer arrays, for internal abdominal organs; high-frequency transducers, for superficial organs such as the skin and thyroid; endocavitary arrays, for prostate or ovary imaging). Aim-

Fig. 5. Two commercially available preclinical photoacoustic imaging systems. (A) The Vevo LAZR-X (VisualSonics, Toronto, ON, Canada) uses intersecting planar laser beams (laser: 680–970 nm and 1,200–2,000 nm). (B) The Nexus 128 (Endra Life Sciences, Ann Arbor, MI, USA) delivers diffuse laser light and detects ultrasound waves using 128 transducers in a helical arrangement for 3-dimensional reconstruction.

Table 2. Typical commercial photoacoustic imaging instruments for preclinical and clinical studies

Instrument	Modality	Advantage	Application
LAZR-X (VisualSonics)	Ultrasound-photoacoustic imaging integrated	Whole-body with sectional PAI options	Preclinical
Nexus 128 (Endra Life Sciences)	Photoacoustic imaging	Fast imaging and high-resolution 3D image reconstruction	Preclinical cancer detection
MSOT (iThera Medical)	Photoacoustic tomography	Real-time, whole-body tomography with body navigations	Preclinical whole-body PAI especially cancer detection and brain imaging
LOUIS-3D (Tomo Wave Laboratories, Inc.)	Photoacoustic imaging with tunable laser switch	The first PAI scanner for SLN dye injection guidance	Preclinical and clinical studies on oncology, vascular angiography, hematology, etc.

PAI, photoacoustic imaging; 3D, 3-dimensional; SLN, sentinel lymph node.

ing at clinical applications, TomoWave Lab Inc. (Houston, TX, USA) developed the LOUISA-3D photoacoustic imaging instrument (Fig. 6). Additionally, the Twente Group, in collaboration with ESAOTE Europe BV, developed a dual-imaging modality in which an ultrasound transducer array and a diode stack laser are combined in a single ultrasound probe connected to a commercially available ultrasound system. The new modality combines the benefits of ultrasonography and photoacoustic imaging by providing anatomic details through ultrasonography and functional information through the photoacoustic imaging.[8] Photoacoustic imaging scanners have been applied in clinics as a prototype for augmenting ultrasound through techniques such as sentinel lymph node (SLN) dye injection. Table 2 shows typical commercial photoacoustic imaging instruments for preclinical and clinical applications.[9]

CLINICAL APPLICATIONS OF PHOTOACOUSTIC IMAGING

The applications of photoacoustic imaging are being inten-

https://doi.org/10.14245/ns.1836206.103

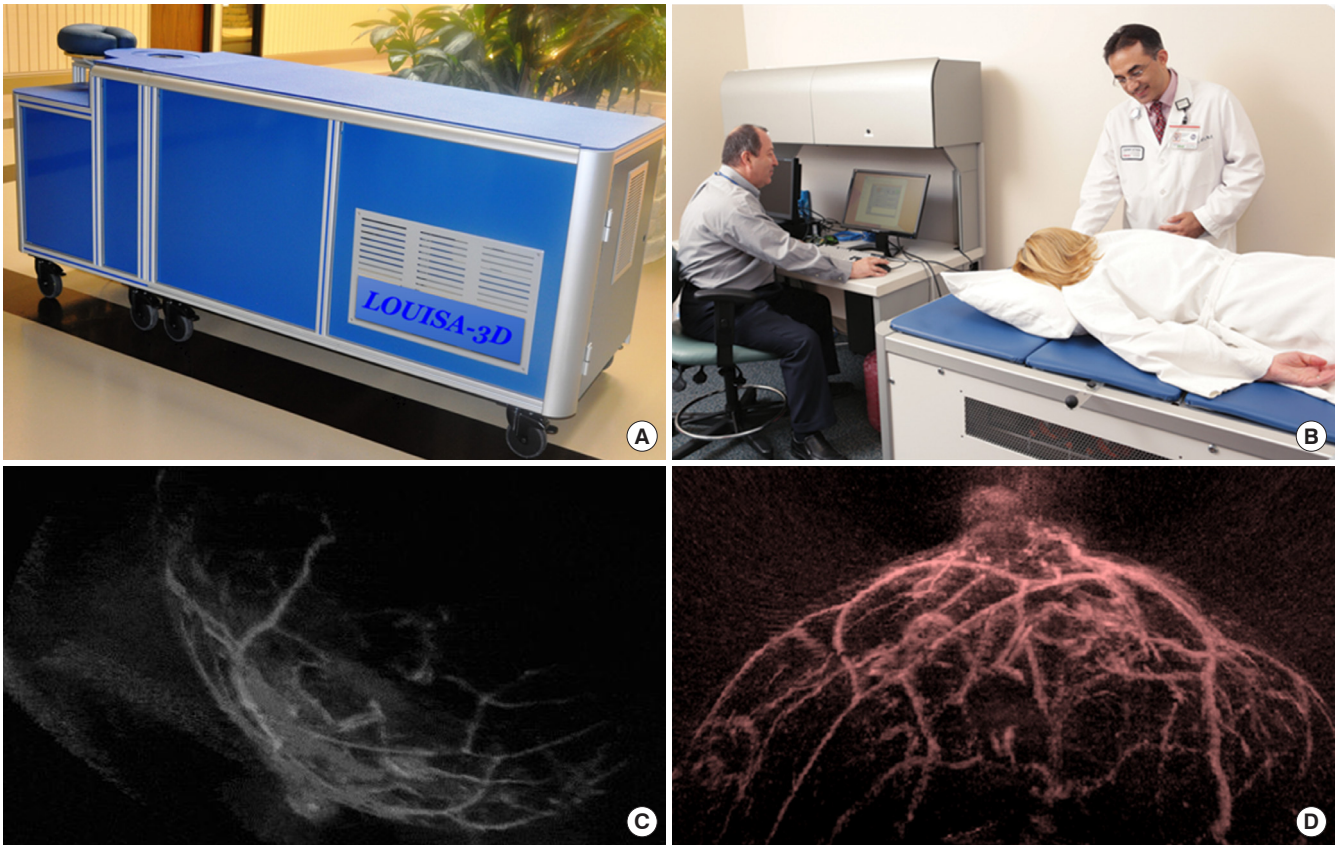

Fig. 6. Clinical photoacoustic imaging systems. (A) LOUISA-3D Photoacoustic Imaging System (TomoWave Lab Inc., Houston, TX, USA). (B) Clinical applications of LOUISA-3D for Breast Imaging. Panels C and D show examples of noninvasive clinical breast imaging with 3-dimensional volumetric images of the breast, along with 2-dimensional ultrasonic images for image coregistration the using LOUISA-3D.

sively studied in fundamental, preclinical, and clinical studies. Many research groups are studying clinical photoacoustic imaging systems. Fig. 7 presents an overview of possible clinical applications of photoacoustic imaging. Several photoacoustic platforms for clinical use already exist or are under development, including handheld probes and photoacoustic computed tomography.

1. Cancer Detection

Photoacoustic imaging is highly promising for cancer monitoring, assessing tumor margins, and screening for tumor metastasis. Several studies have explored photoacoustic breast imaging as a possible alternative to X-ray mammography. Typically, photoacoustic mammography systems include a patient examination table that contains an aperture through which the patient's breast is suspended while lying in prone position. A laser and detector are arranged underneath the examination table, and imaging is conducted with the breast mildly compressed. An example of such a system is the photoacoustic mammoscope, which was developed at the University of Twente (Enschede, The Netherlands) as a clinical prototype.[10] This system utilizes a 2-dimensional circular ultrasound detector array (80-mm diameter, 590 elements, 1-MHz center frequency) on one side of the compressed breast with laser exposure (1,064 nm, 10 mJ/cm^2) from the other side to facilitate 3-dimensional imaging. A clinical study was recently conducted (Fig. 8) of 43 patients, who had 31 malignant lesions, 2 fibroadenomas, 1 area of chronic inflammation, 5 cysts, and 2 invalid measurements. The tumors were visualized with high contrast in 30 of the 31 breast cancer patients (Breast Imaging Reporting and Data System density: low [1 or 2] in 23 patients and high [3 or 4] in 8 patients). On the basis of these findings, it was concluded that the photoacoustic image contrast was independent of the breast density estimated on mammography, unlike X-ray mammography.[11] The average scan time with the photoacoustic mammoscope was 10 minutes for a field of view of 90×80 mm.[2]

In addition to detecting primary tumors, screening for metastasis is another important application of clinical imaging.

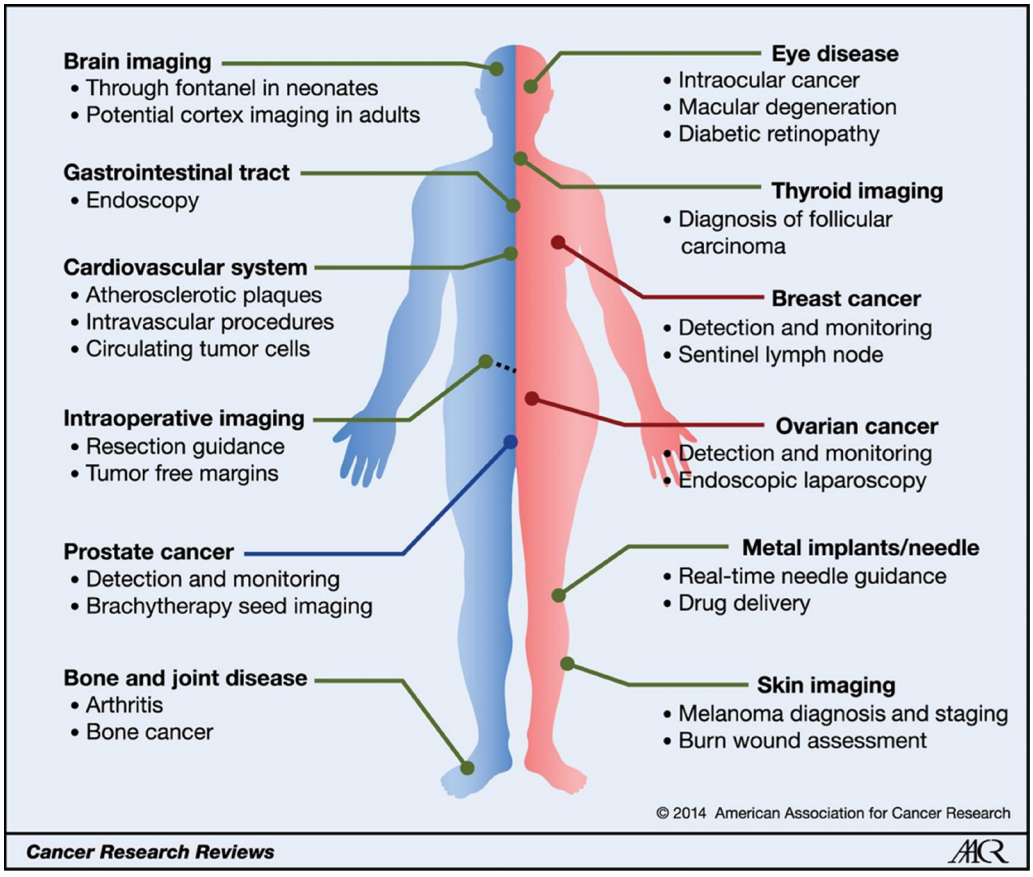

Fig. 7. Overview of the potential clinical applications of photoacoustic imaging. Overview of potential clinical applications of photoacoustic imaging. The main possible applications for each organ system are listed. Some of these applications are male-specific (left, blue line), and some are female-specific (right, red line).[51]

Early-stage metastasis always occurs in the SLNs, which comprise a tumor bed that receives lymphatic drainage from cancerous tissues.[12,13] By using an exogenous agent, such as methylene blue or indocyanine green (ICG), photoacoustic imaging has been used to detect SLNs deep in tissues. The absence of endogenous photosensitive molecules in lymph nodes has led researchers to use exogenous photoacoustic imaging contrast agents. In an *in vivo* rat study, Song et al.[14] successfully imaged SLNs with a photoacoustic imaging system using methylene blue, an optically absorbing contrast agent. Fig. 9 presents an ICG-stained SLN photoacoustic image.[15]

Some researchers have studied photoacoustic imaging of prostate cancer *in vivo* using animal models.[16-20] Levi et al. developed a photoacoustic contrast agent labeled AA3G-740 that binds to gastrin-releasing peptide receptor, which has been reported to be highly overexpressed in prostate cancer.[21,22] *In vivo* molecular photoacoustic imaging of mice (n = 6) bearing PC3 human prostate cancer cells was performed 30 and 60 minutes after contrast agent injection using the Nexus 128 photoacoustic computed tomography system (Endra Life Sciences). AA3G-740 was able to bind to gastrin-releasing peptide receptor in mice, even in poorly vascularized tumors, leading to a nearly twofold increase in the photoacoustic signal relative to a control contrast agent.[22] It was also reported that the smallest number of AA3G-740–labeled PC3 cells required to produce a background-differentiable photoacoustic signal was only 0.5 million (whereas a 1-cm^3 tumor may have up to 100 million cells), which demonstrates the potential of molecular photoacoustic imaging to detect prostate cancer, even in small tumors.

Aguirre et al.[23] developed a coregistered photoacoustic and ultrasound imaging system suitable for *ex vivo* ovarian imaging. This system uses a tunable laser (740 nm, 12 ns, 15 Hz) and a custom-developed 1.75-dimensional transducer array (5 MHz). With this system, an *ex vivo* study was performed on 33 human ovaries that were extracted from patients who underwent oophorectomy. This system showed the capability to differentiate normal postmenopausal versus malignant postmenopausal ovaries (p = 0.0237) (sensitivity, 83%; specificity, 83%). In contrast,

 https://doi.org/10.14245/ns.1836206.103

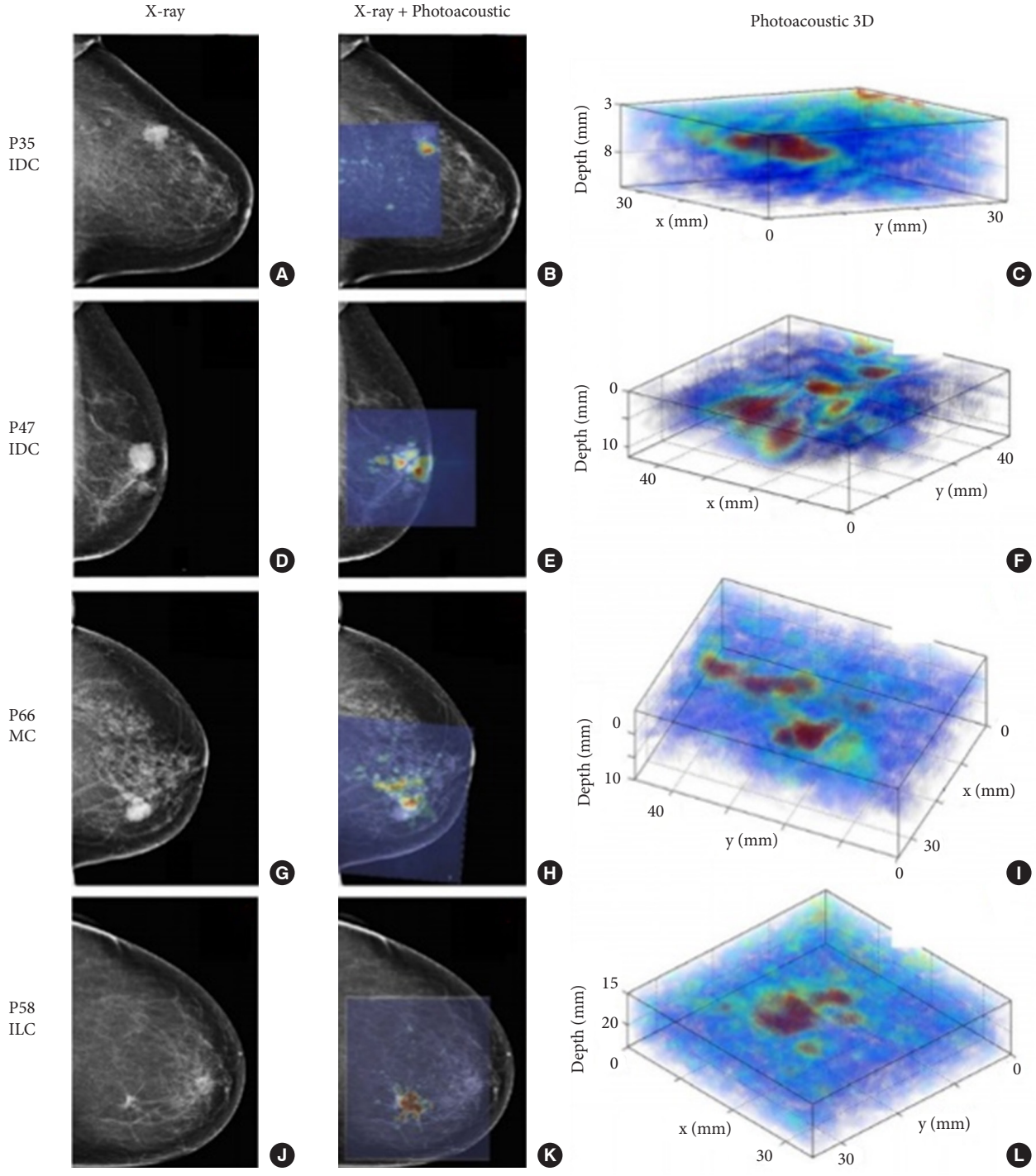

Fig. 8. Breast imaging with photoacoustic mammoscope. Photoacoustic images were overlaid on X-ray mammograms to show lesions detected on both modalities. Reconstructed 3-dimensional (3D) photoacoustic volume encompassing each lesion of interest is also shown here. Infiltrating ductal carcinoma (IDC) lesion was seen on X-ray and photoacoustic imaging in a 79-year-old patient (A-C) and a 69-year-old patient (D-F), respectively. Mucinous carcinoma (MC) was detected in an 83-year-old patient (G-I) while infiltrating lobular carcinoma (ILC) was seen in a 65-year-old patient (J-L). The lesions were co-localized on photoacoustic images with respect to X-ray mammograms and were visualized at depths of more than 20 mm with good contrast on photoacoustic images. PXX indicates patient-identifier in the study. Reproduced from Heijblom et al.[11] Eur Radiol 2016;26:3874-87, according to the Open Access.

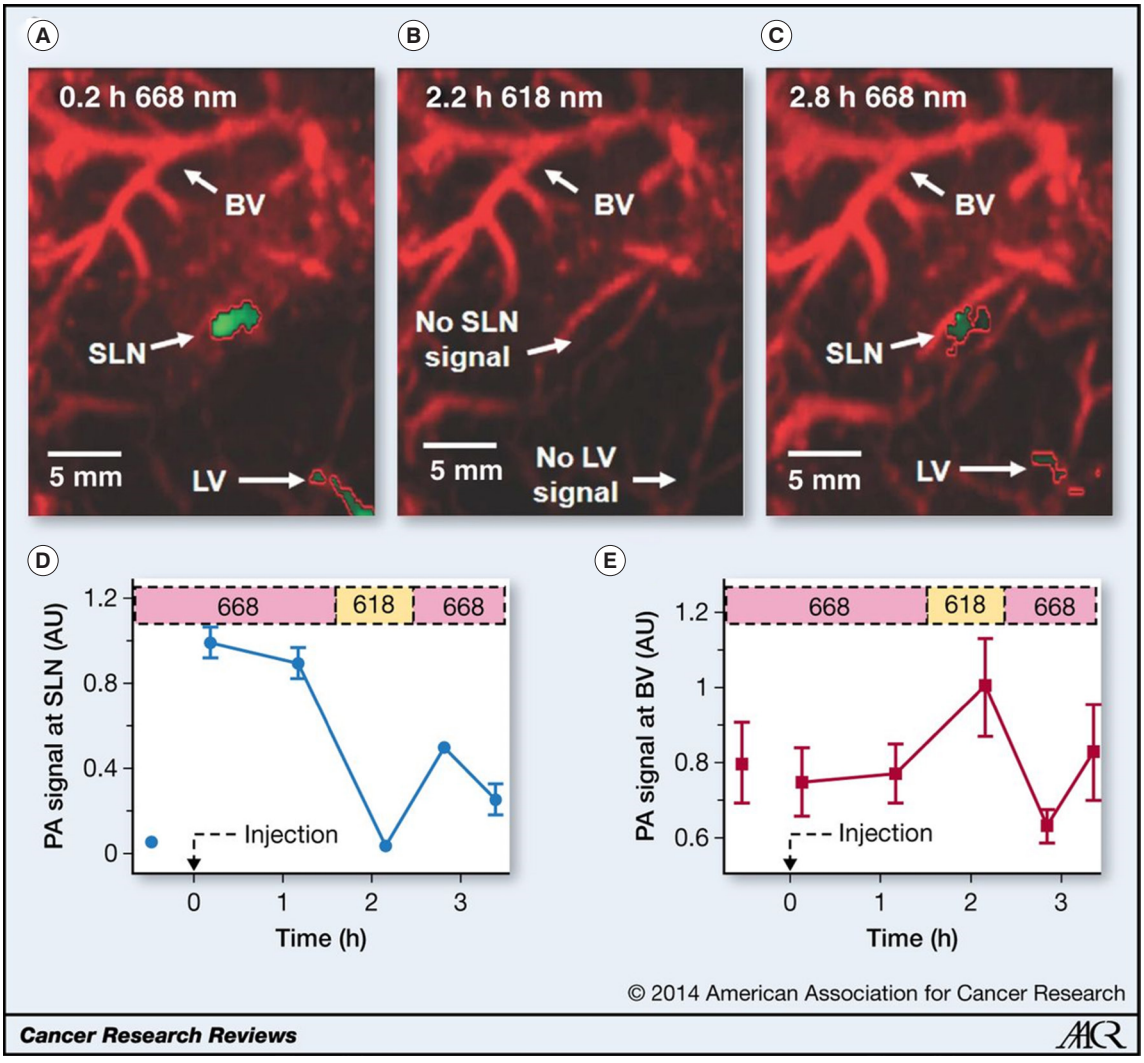

Fig. 9. Photoacoustic images of sentinel lymph node (SLN) in a rat *in vivo* after indocyanine green (ICG) injection. (A) Image at 668 nm 0.2 hours after ICG injection. (B) Image at 618 nm 2.2 hours after injection. (C) Image at 668 nm 2.8 hours after injection. (D) Graph shows comparison of spectroscopic photoacoustic signals within the SLN region over a period of time. (E) Graph shows comparison of spectroscopic photoacoustic signals within blood vessels (BVs) over a period of time. LV, lymphatic vessel. Numbers in colored bar at top of panels D and E equal wavelength in nanometers. Reprinted from Kim et al.[15] Radiology 2010;255:442-50, with permission of The Radiological Society of North America.

no significant differences were found between normal premenopausal versus normal postmenopausal ovaries ($p = 0.2361$) (Fig. 10). The same research group[24,25] later reported an upgraded system built specifically for clinical use that employed a laser (750 nm, 20 ns, 15 Hz) and a modified commercial transvaginal ultrasound probe (6 MHz), around which an array of 36 optical fibers was mounted to facilitate *in vivo* photoacoustic imaging.

2. Imaging-guided Surgery

IGS refers to real-time correlation of the operative field with preoperative imaging data in order to determine the precise location of a selected surgical instrument relative to the surrounding anatomic structures. IGS has become recognized as a way for surgeons to perform safer, less invasive surgery in the fields of intracranial otolaryngology, spine, orthopedics and cardiovascular disease. Some researchers have shown that photoacoustic imaging enables real-time visualization of areas of interest during surgery. This is significant because it is more difficult to perform surgery with static reference images (e.g., computed tomography scans and magnetic resonance images) of internal structures, although surgeons typically use such images to visu-

https://doi.org/10.14245/ns.1836206.103

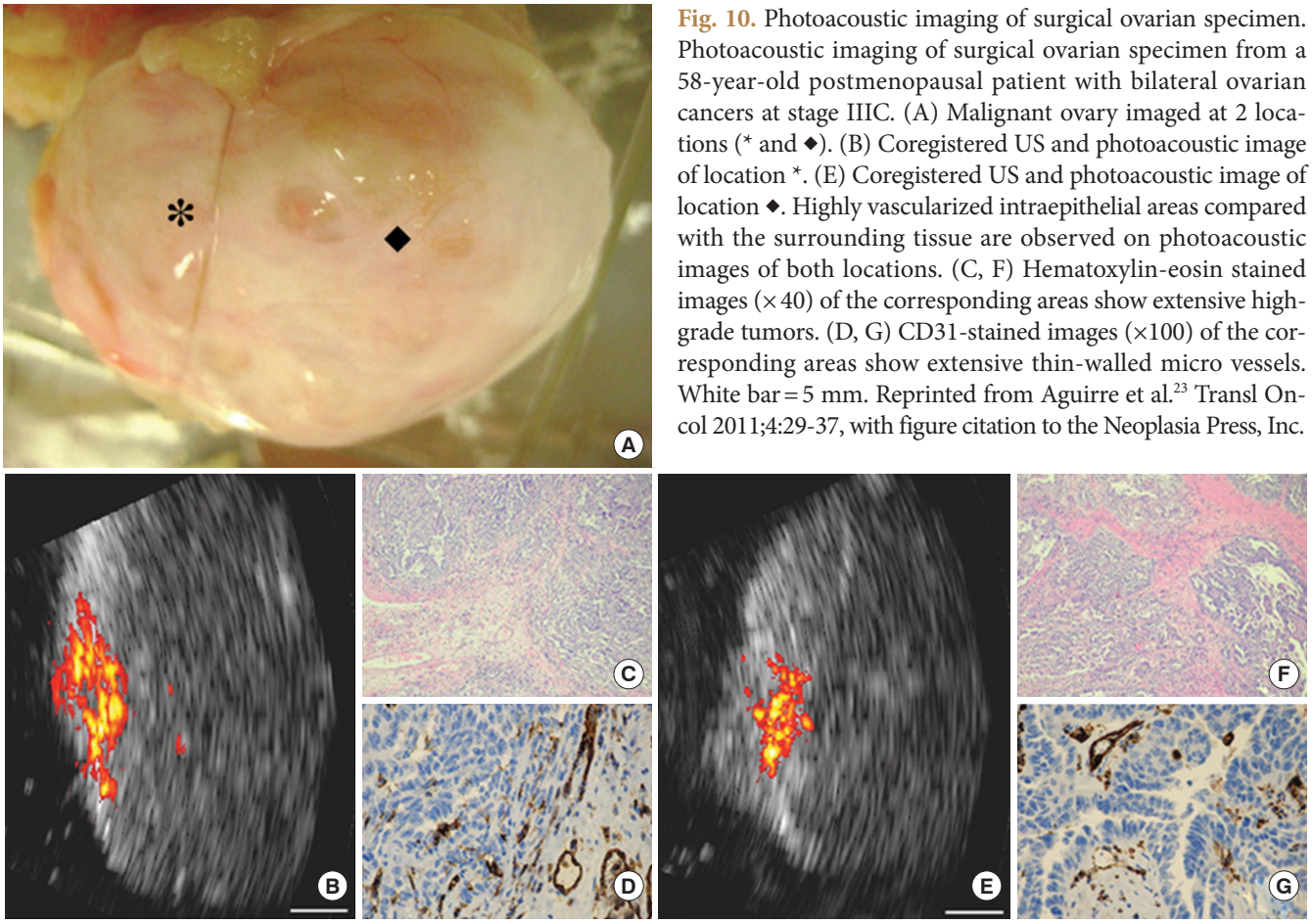

Fig. 10. Photoacoustic imaging of surgical ovarian specimen. Photoacoustic imaging of surgical ovarian specimen from a 58-year-old postmenopausal patient with bilateral ovarian cancers at stage IIIC. (A) Malignant ovary imaged at 2 locations (* and ◆). (B) Coregistered US and photoacoustic image of location *. (E) Coregistered US and photoacoustic image of location ◆. Highly vascularized intraepithelial areas compared with the surrounding tissue are observed on photoacoustic images of both locations. (C, F) Hematoxylin-eosin stained images (×40) of the corresponding areas show extensive high-grade tumors. (D, G) CD31-stained images (×100) of the corresponding areas show extensive thin-walled micro vessels. White bar = 5 mm. Reprinted from Aguirre et al.[23] Transl Oncol 2011;4:29-37, with figure citation to the Neoplasia Press, Inc.

alize targets hidden by bone and other tissues.[2] Studies of intraoperative photoacoustic imaging remain in their early stages. Xi et al.[26] reported a microelectromechanical system using intraoperative photoacoustic tomography and examined the capability of this system to map tumors accurately in 3 dimensions and to inspect the completeness of tumor resection during surgery in a tumor-bearing mouse model.

IGS can help surgeons perform minimally invasive percutaneous, laparoscopic, or robotic-aided treatment more precisely and safely, to achieve complete tumor removal, and to preserve of the function of critical organs. Recently, with the advent of minimally invasive treatment procedures, surgical procedures have tended to shift from large-scale exploration to approaches with limited access and limited visibility. These new applications increase the need for image guidance and mandate the use of the most advanced imaging methods. Some research groups are exploring systems for delivering light surrounding surgical tools, with applications to minimally invasive surgery, such as neurosurgical procedures to remove pituitary tumors using the endonasal transsphenoidal approach. In this approach, the light delivery system would be attached to the surgical tool, which is inserted in the nose, and would transmit light across the sphenoid bone. The internal carotid arteries hidden behind the bone would absorb the light, undergo thermal expansion, and generate an acoustic response to be detected by an external transcranial ultrasound probe placed on the patient's temple.[27] The Photoacoustic & Ultrasonic Systems Engineering (PULSE) Lab at Johns Hopkins University has been investigating the use of photoacoustic imaging for minimally invasive IGS.[2,27] Bell and colleagues[2,27-29] have reported the application of photoacoustic imaging for real-time surgical guidance. They provided an overview of the combination of photoacoustic imaging with the da Vinci surgical robot, which is often used to perform teleoperated hysterectomies (i.e., surgical removal of the uterus).[30] A concerning complication of hysterectomies is accidental injury of the ureters, which are located within millimeters of the uterine arteries that are severed and cauterized to hinder blood flow and enable full removal of the uterus. The researchers explored the possibility that photoacoustic imaging could visualize the uterine arteries (and potentially the ureters) during hysterecto-

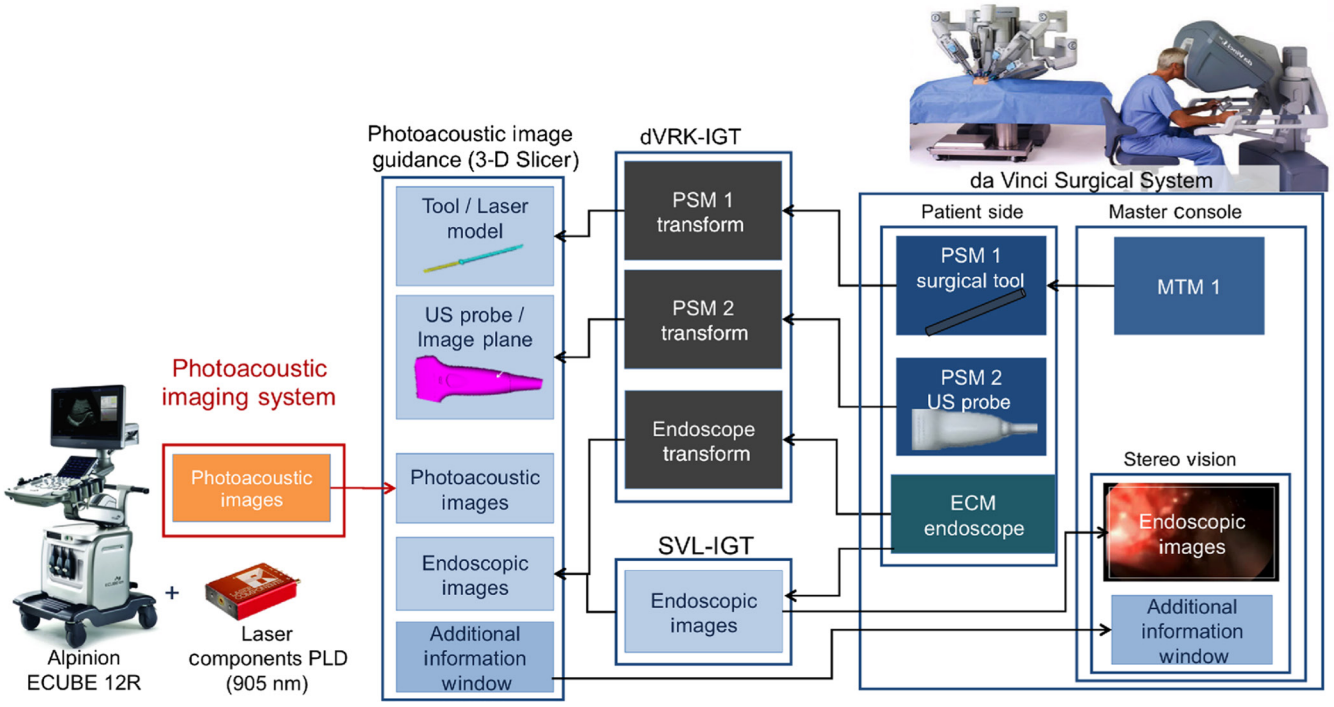

Fig. 11. Integrated system architecture with photoacoustic imaging and robotic surgery system. Photoacoustic images are generated and sent to the photoacoustic image guidance module (via a 3-D slicer plug-in) for visualization, along with live stereo endoscope video (via SVL-IGT) and models of the drill, laser, and ultrasound probe that are positioned based on kinematic position feedback from the da Vinci patient-side manipulators (via dVRK-IGT). Visualizations from the 3-D Slicer are sent to the da Vinci stereo viewer. SVL, cisst Stereo Vision Library27; dVRK, da Vinci Research Kit;[31] PLD, pulsed laser diode; 3-D, three-dimensional; IGT, image-guided therapy; PSM, patient side manipulators; ECM, endoscopic camera manipulator; MTM, master tool manipulator.

my. Photoacoustic images were obtained while sweeping the tool across a custom 3-dimensional uterine vessel model covered in *ex vivo* bovine tissue that was placed between the 3-dimensional model and the light delivery system, as well as between the ultrasound probe and the 3-dimensional model (to introduce optical and acoustic scattering). Fig. 11 shows how the photoacoustic imaging system was interfaced with the da Vinci Robot surgical system for teleoperation of the imaging system components, facilitated by the da Vinci research toolkit.[31]

3. Other Applications

Most recently, photoacoustic imaging been broadly applied in fields ranging from functional brain mapping and cancer diagnosis to tissue engineering, surgery, drug delivery, and cell biology, as has been reviewed in depth elsewhere.[32] In addition to the above-discussed applications of cancer diagnosis and surgery, we will introduce the application of photoacoustic imaging for related to brain and bone imaging in neuroscience. Photoacoustic tomography provides important information about the cerebral vasculature by enabling functional and metabolic brain imaging on both the microscopic and macroscopic scales,[32] yielding information about oxygenation (Fig. 12),[33] the metabolism of oxygen and glucose,[34] resting-state connectivity,[35] and how the brain responds to various physiological and pathological challenges.[36-38] Photoacoustic tomography can be used for neuronal imaging, using either exogenous contrast from dyes or endogenous contrast from lipids.[39] In addition, photoacoustic tomography has been increasingly used to study small-animal models of brain diseases, including stroke,[40] epilepsy,[41] and edema.[42] Recently, head-mounted photoacoustic computed tomography systems have been developed, which is an important step toward functional photoacoustic imaging of the brain in free-moving animals.[43] Van den Berg et al.[44] developed a dual-modality photoacoustic imaging system with a handheld probe for assessing synovitis in patients with rheumatoid arthritis. As shown in Fig. 13, the probe contains a fully assembled ultrasound transducer and a compact diode laser module in a size comparable to that of commercially-available ultrasound imaging probes used in current clinical practice.[45] The photoacoustic

 https://doi.org/10.14245/ns.1836206.103

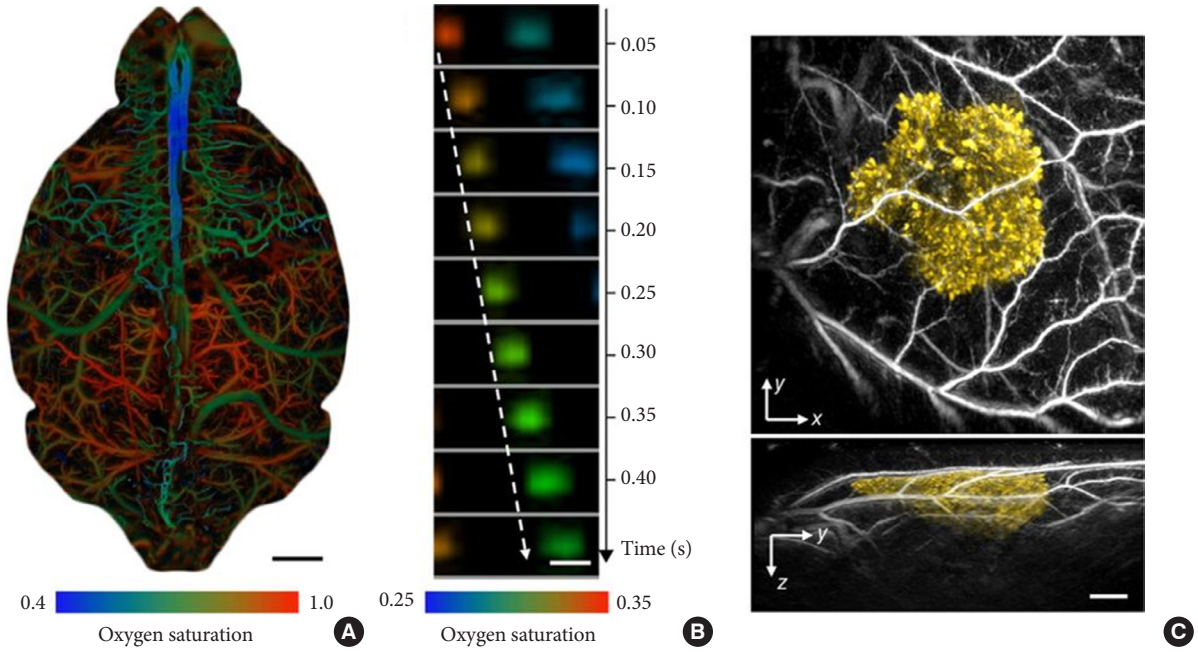

Fig. 12. Representative in vivo photoacoustic tomography applications in life sciences. (A) Whole-cortex optical-resolution photoacoustic microscopy (OR-PAM) image of the oxygen saturation of hemoglobin in a mouse brain.[52] The arteries (shown in red) and veins (shown in blue/green) are clearly differentiated by their oxygenation levels. Blue indicates low oxygenation. Scale bar, 1 mm. (B) Sequential label-free OR-PAM images of oxygen releasing in single red blood cells (RBCs) flowing in a capillary in a mouse brain.[53] Scale bar, 10 μm. Blood flows from left to right. The dashed arrow follows the trajectory of a single flowing RBC. (C) Photoacoustic computed tomography images of a tyrosinase-expressing K562 tumor (shown in yellow) after subcutaneous injection into the flank of a nude mouse.[54] The surrounding blood vessels are shown in gray. Top, x-y projection image; bottom, y-z projection image. Scale bar, 1 mm.

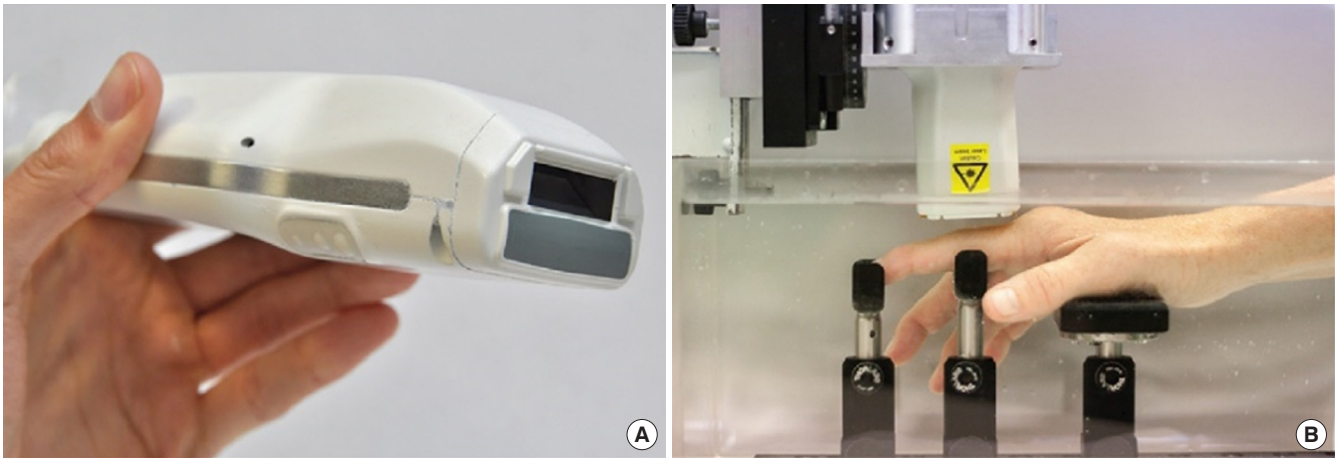

Fig. 13. A probe that houses both a small diode laser together with ultrasound transducers. The photoacoustic imaging/ultrasound probe (A) with a view of the front end showing the light delivery window (dark aperture) and acoustic lens in medium gray. The patient's hand is submerged in water (B) where it rests on a series of supports. The probe is mounted on a 2-axis motorized stage and positioned above the joint.

images in Fig. 14A show a superficial blood vessel in both the inflamed and non-inflamed joints, with additional photoacoustic findings on the bone surface. The inflamed joint shows larger amplitudes and more confluent features, as can be further observed in Fig. 14B, where only high amplitudes (18-dB dynamic range) are plotted. With this threshold, almost no photo-

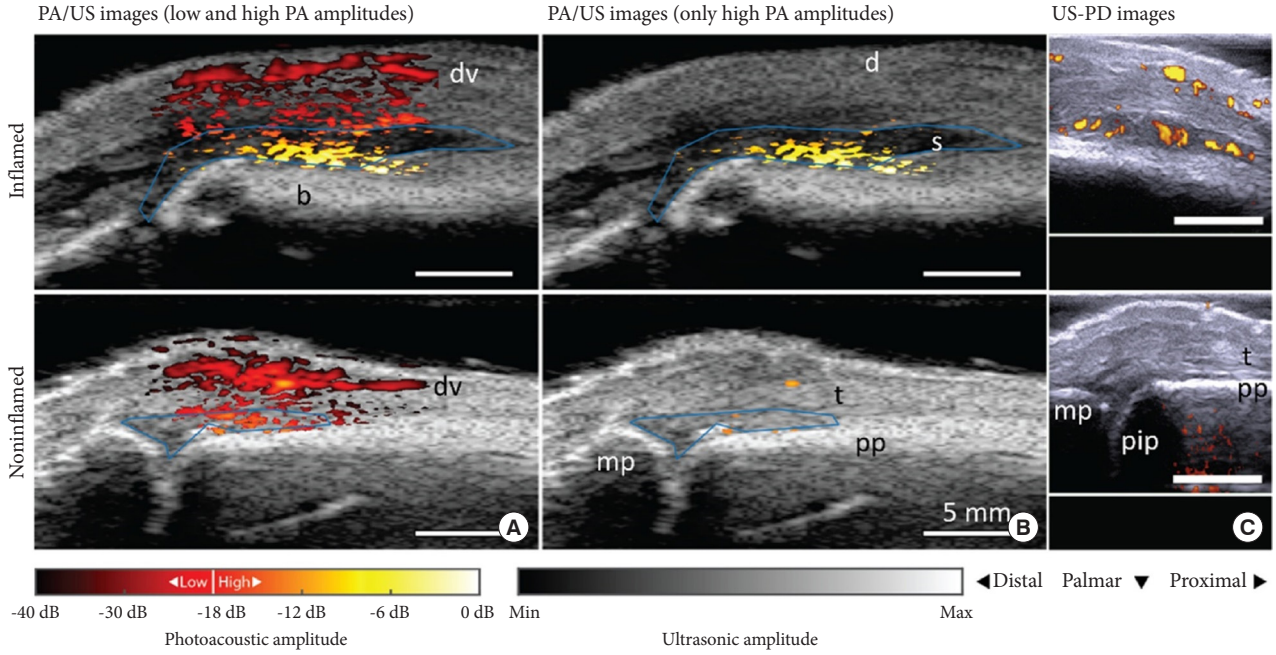

Fig. 14. Examples of fluence-corrected photoacoustic imaging/ultrasound and US-PD images for an inflamed joint and the contra-lateral noninflamed joint. Photoacoustic imaging/ultrasound and US/PD images of an inflamed (upper row) and noninflamed contralateral joint (bottom row) of a rheumatoid arthritis (RA) patient. The photoacoustic imaging/ultrasound images in panel A show a difference in color between the inflamed and noninflamed joints corresponding to an increase in amplitude levels. When discarding the low photoacoustic amplitudes in panel B, only features in the inflamed joint are visible. The corresponding US-PD images are shown in panel C. The blue line in the PA/US images indicates the region of interest used for quantification of photoacoustic imaging features in the synovial space. The 0-dB level is the maximum photoacoustic imaging amplitude from the inflamed joint. US-PD, ultrasound power doppler; PA/US, photoacoustic/ultrasound; d, dermis; dv, dorsal vein; pp, proximal phalanx; pip, proximal interphalangeal joint; mp, middle phalanx; s, synovium; t, extensor tendon.

acoustic features are visible for the noninflamed joint.[44]

APPLICATIONS OF PHOTOACOUSTIC IMAGING FOR SPINAL SURGERY

Thella et al.[46] demonstrated that photoacoustic imaging shows potential for the noninvasive diagnosis of various bone types, including bones containing cancer. In addition, photoacoustic technology has been found to be sensitive to minor variations in cortical bone density.[47] Quantitative photoacoustic imaging has been further used to determine differences in bone mineral density and bone composition,[48,49] which could be useful for preventing spinal injury and choosing a suitable starting point prior to drilling or insertion of a spinal probe. However, to the best of the authors' knowledge, photoacoustic images of the pedicles in a human vertebra have never been published, meaning that a clinically viable photoacoustic imaging approach to guide spinal fusion surgery has never been explored. In 2018, Shubert and Lediju Bell[50] published a paper about spinal surgery using photoacoustic imaging, exploring the possibility of using photoacoustic imaging to differentiate between cortical and cancellous bone, with implications for possible use for guidance in spinal fusion surgery. For deployment as a viable clinical system, the optical fiber carrying the laser light can be detached or attached to surgical instruments (e.g., a burr, drill, awl, or spinal probe). Next, a standard clinical ultrasound probe would be placed on the vertebra of interest with acoustic coupling gel. They have shown that it was possible to use photoacoustic imaging to differentiate cancellous and cortical bone without drilling or otherwise disrupting the pedicle. This finding suggests that photoacoustic imaging has the clinical potential to generate signals from the cancellous core of the pedicle prior to the removal of any surface cortical bone. With photoacoustic imaging used to determine the starting point, the findings presented in Figs. 15 and 16 indicate that a smaller probe-fiber pair that fits inside a predrilled hole may also be used as a real-time indicator of the optimal trajectory of the drill or pedicle probe. Their study was the first to show that 3-dimensional

https://doi.org/10.14245/ns.1836206.103

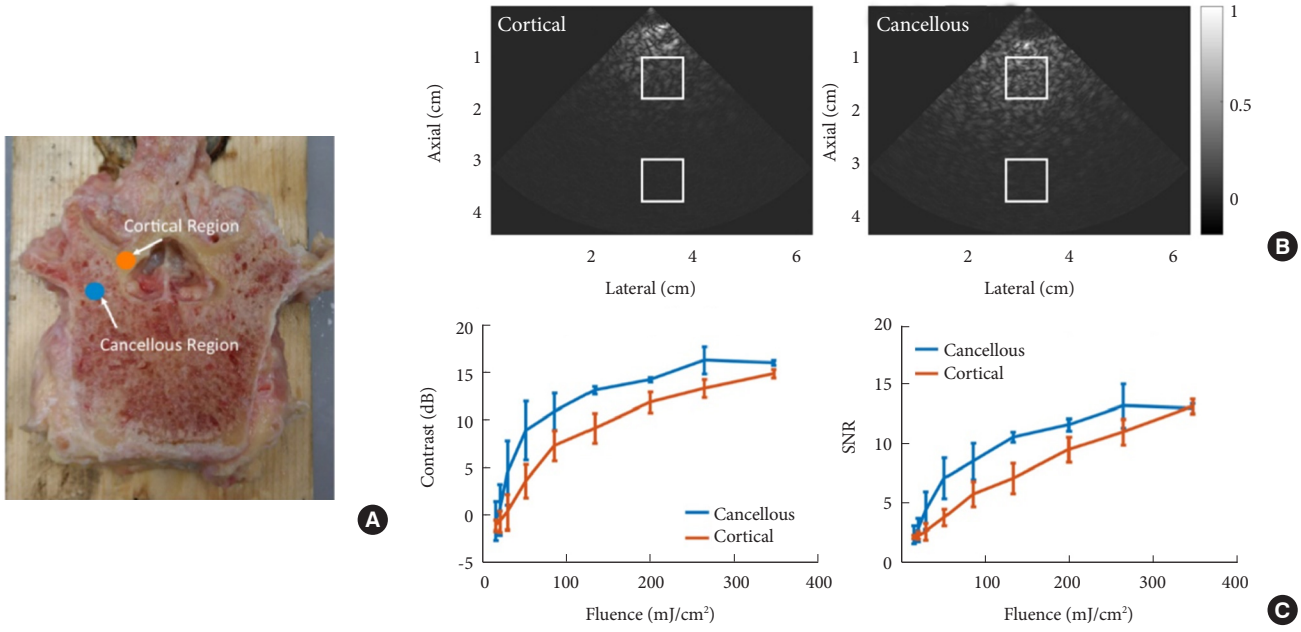

Fig. 15. Photoacoustic imaging of a human vertebra: implications for guiding spinal fusion surgery. (A) Photograph annotated with the location of fiber-probe pair for contrast and signal-to-noise ratio (SNR) measurements. (B) Examples of photoacoustic images and fixed region of interest locations for contrast and SNR measurements, acquired with 200 mJ cm^{-2} laser fluence. (C) Contrast and SNR as a function of laser fluence. Plots show mean ± standard deviation values for 15 measurements.

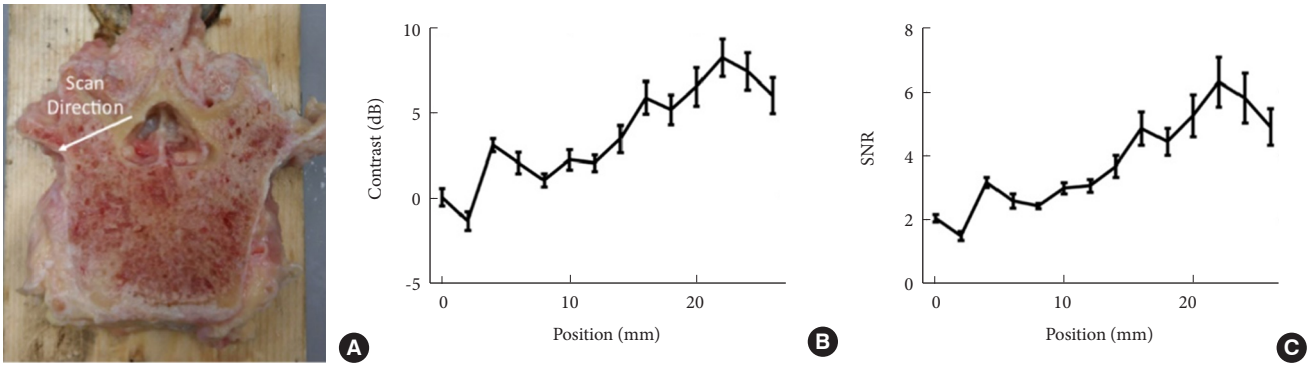

Fig. 16. Differences in signal contrast and the signal-to-noise ratio (SNR) as a function of distance from the cortical region. (A) Photograph annotated with the scanning direction of the fiber-probe pair. Contrast (B) and SNR (C) as a function of the position of the optical fiber, which was attached to the phased-array ultrasound probe. Plots show mean ± standard deviation values for 15 measurements.

photoacoustic imaging could be used as a noninvasive technique to reveal differences between cancellous and cortical bone, indicating that this modality is promising for spinal fusion surgery.

CONCLUSION

Photoacoustic imaging is a promising imaging modality used for cancer diagnosis, surgery, drug delivery, brain imaging, and inflammatory arthritis, as a complement to existing imaging modalities. In this review, we presented several instruments used for photoacoustic imaging and described selected clinical applications, including spinal surgery. Although photoacoustic imaging has many potential applications, several challenges remain, as we discussed. In the field of spinal surgery, the first steps have been taken in studying the use of photoacoustic imaging for IGS. This initial work generally shows promise for the potential of photoacoustic imaging systems to overcome a wide range of longstanding challenges in spinal surgery, including

the occurrence of bone breaches due to misplaced pedicle screws. To surmount these challenges, many institutions and researchers are developing novel approaches regarding laser sources, ultrasound transducers, multimodal platforms, and detector geometry, and are exploring potential applications.

CONFLICT OF INTEREST

The author has nothing to disclose.

ACKNOWLEDGMENTS

The author acknowledges helpful discussions with and contributions from members of Brian Wilson's Bio-photonics Group in the University Health Network.

REFERENCES

1. Jolesz FA. Definition of image guided therapy. In: Jolesz FA, editor. Intraopeative imaging and image-guided therapy. New York: Springer; 2014. p. 1-23.
2 Eddins B, Bell MA. Design of a multifiber light delivery system for photoacoustic-guided surgery. J Biomed Opt 2017; 22:41011.
3. Bell AG. On the production and reproduction of sound by light. Am J Sci 1880;20:305-24.
4. Wang LV. Tutorial on photoacoustic microscopy and computed tomography. IEEE J Sel Top Quantum Electron 2008; 14:171-9.
5. Beard P. Biomedical photoacoustic imaging. Interface Focus 2011;1:602-31.
6. Rao NA. Ultrasound imaging. Hoboken (NJ): John Wiley & Sons; 2002.
7. Valluru KS, Willmann JK. Clinical photoacoustic imaging of cancer. Ultrasonography 2016;35:267-80.
8. Singh MK, Steenbergen W, Manohar S. Handheld probe-based dual mode ultrasound/photoacoustics for biomedical imaging. In: Olivo M, Dinish US, editors. Frontiers in biophotonics for translational medicine in the celebration of year of light (2015). Singapore: Springer; 2015. p. 209-47.
9. Zou C, Wu B, Dong Y, et al. Biomedical photoacoustics: fundamentals, instrumentation and perspectives on nanomedicine. Int J Nanomedicine 2016;12:179-95.
10. Piras D, Xia W, Steenbergen W, et al. Photoacoustic imaging of the breast using the twente photoacoustic mammoscope: present status and future perspectives. IEEE J Sel Top Quantum Electron 2010;16:730-9.
11. Heijblom M, Piras D, van den Engh FM, et al. The state of the art in breast imaging using the Twente Photoacoustic Mammoscope: results from 31 measurements on malignancies. Eur Radiol 2016;26:3874-87.
12. Wittekind C, Neid M. Cancer invasion and metastasis. Oncology 2005;69 Suppl 1:14-6.
13. Veronesi U, Paganelli G, Galimberti V, et al. Sentinel-node biopsy to avoid axillary dissection in breast cancer with clinically negative lymph-nodes. Lancet 1997;349:1864-7.
14. Song KH, Stein EW, Margenthaler JA, et al. Noninvasive photoacoustic identification of sentinel lymph nodes containing methylene blue in vivo in a rat model. J Biomed Opt 2008;13:054033.
15. Kim C, Song KH, Gao F, et al. Sentinel lymph nodes and lymphatic vessels: noninvasive dual-modality in vivo mapping by using indocyanine green in rats--volumetric spectroscopic photoacoustic imaging and planar fluorescence imaging. Radiology 2010;255:442-50.
16. Wang X, Roberts WW, Carson PL, et al. Photoacoustic tomography: a potential new tool for prostate cancer. Biomed Opt Express 2010;1:1117-26.
17. Olafsson R, Bauer DR, Montilla LG, et al. contrast enhanced photoacoustic imaging of cancer in a mouse window chamber. Opt Express 2010;18:18625-32.
18. Bauer DR, Olafsson R, Montilla LG, et al. 3-D photoacoustic and pulse echo imaging of prostate tumor progression in the mouse window chamber. J Biomed Opt 2011;16:026012.
19. Yaseen MA, Brecht HP, Ermilov SA, et al. Hybrid optoacoustic and ultrasonic imaging system for detection of prostate malignancies. In: Proceedings of SPIE - The International Society for Optical Engineering 6856. 2008;6856:68560T-2.
20. Yaseen MA, Ermilov SA, Brecht HP, et al. Optoacoustic imaging of the prostate: development toward image-guided biopsy. J Biomed Opt 2010;15:021310.
21. Agarwal A, Huang SW, O'Donnell M, et al. Targeted gold nanorod contrast agent for prostate cancer detection by photoacoustic imaging. J Appl Phys 2007;102:064701.
22. Levi J, Sathirachinda A, Gambhir SS. A high-affinity, high-stability photoacoustic agent for imaging gastrin-releasing peptide receptor in prostate cancer. Clin Cancer Res 2014; 20:3721-9.
23. Aguirre A, Ardeshirpour Y, Sanders MM, et al. Potential role of coregistered photoacoustic and ultrasound imaging in ovarian cancer detection and characterization. Transl Oncol 2011;4:29-37.

 https://doi.org/10.14245/ns.1836206.103

24. Kumavor PD, Alqasemi U, Tavakoli B, et al. Co-registered pulse-echo/photoacoustic transvaginal probe for real time imaging of ovarian tissue. J Biophotonics 2013;6:475-84.
25. Alqasemi U, Li H, Yuan G, et al. Ultrafast ultrasound and photoacoustic co-registered imaging system based on FPGA parallel processing. In: Oraevsky AA, Wang LV, editors. Proceedings of SPIE: medical imaging 2012—photons plus ultrasound: imaging and sensing 2012. Bellingham (WA): International Society for Optics and Photonics; 2012:82232U.
26. Xi L, Grobmyer SR, Wu L, et al. Evaluation of breast tumor margins in vivo with intraoperative photoacoustic imaging. Opt Express 2012;20:8726-31.
27. Lediju Bell MA, Ostrowski AK, Li K, et al. Localization of transcranial targets for photoacoustic-guided endonasal surgeries. Photoacoustics 2015;3:78-87.
28. Gandhi N, Allard M, Kim S, et al, Photoacoustic-based approach to surgical guidance performed with and without a da Vinci robot. J Biomed Opt 2017;22:121606.
29. Allard M, Shubert J, Bell MAL. Feasibility of photoacoustic-guided teleoperated hysterectomies. J Med Imaging (Bellingham) 2018;5:021213.
30. Allard M, Shubert J, Lediju Bell MA. Technical note: feasibility of photoacoustic guided hysterectomies with the da Vinci robot. Proceedings Volume 10576, Medical Imaging 2018: image-guided procedures, robotic interventions, and modeling; 105760A; 2018 Mar 12; Houston (TX), USA. https://doi.org/10.1117/12.2293176.
31. Kazanzidesy P, Chen Z, Deguet A, et al. An open-source research kit for the da Vinci® Surgical System. In: 2014 IEEE International Conference on Robotics & Automation (ICRA); 2014 May 31-Jun 7; Hong Kong. IEEE 2014:6434-9.
32. Laufer J, Zhang E, Raivich G, et al. Three-dimensional noninvasive imaging of the vasculature in the mouse brain using a high resolution photoacoustic scanner. Appl Opt 2009; 48:D299-306.
33. Burton NC, Patel M, Morscher S, et al. Multispectral opto-acoustic tomography (MSOT) of the brain and glioblastoma characterization. Neuroimage 2013;65:522-8.
34. Yao J, Xia J, Maslov KI, et al. Noninvasive photoacoustic computed tomography of mouse brain metabolism in vivo. Neuroimage 2013;64:257-66.
35. Nasiriavanaki M, Xia J, Wan H, et al. High-resolution photoacoustic tomography of resting-state functional connectivity in the mouse brain. Proc Natl Acad Sci U S A 2014; 111:21-6.
36. Jo J, Yang X. Functional photoacoustic imaging to observe regional brain activation induced by cocaine hydrochloride. J Biomed Opt 2011;16:090506.
37. Liao LD, Li ML, Lai HY, et al. Imaging brain hemodynamic changes during rat forepaw electrical stimulation using functional photoacoustic microscopy. Neuroimage 2010;52:562-70.
38. Pilatou MC, Marani E, de Mul FF, et al. Photoacoustic imaging of brain perfusion on albino rats by using evans blue as contrast agent. Arch Physiol Biochem 2003;111:389-97.
39. Yao J, Wang LV. Photoacoustic brain imaging: from microscopic to macroscopic scales. Neurophotonics 2014;1.
40. Deng Z, Wang Z, Yang X, et al. In vivo imaging of hemodynamics and oxygen metabolism in acute focal cerebral ischemic rats with laser speckle imaging and functional photoacoustic microscopy. J Biomed Opt 2012;17:081415-1.
41. Tsytsarev V, Rao B, Maslov KI, et al. Photoacoustic and optical coherence tomography of epilepsy with high temporal and spatial resolution and dual optical contrasts. J Neurosci Methods 2013;216:142-5.
42. Xu Z, Zhu Q, Wang LV. In vivo photoacoustic tomography of mouse cerebral edema induced by cold injury. J Biomed Opt 2011;16:066020.
43. Tang J, Xi L, Zhou J, et al. Noninvasive high-speed photoacoustic tomography of cerebral hemodynamics in awake-moving rats. J Cereb Blood Flow Metab 2015;35:1224-32.
44. van den Berg PJ, Daoudi K, Bernelot Moens HJ, et al. Feasibility of photoacoustic/ultrasound imaging of synovitis in finger joints using a point-of-care system. Photoacoustics 2017;8:8-14.
45. Daoudi K, van den Berg PJ, Rabot O, et al. Handheld probe integrating laser diode and ultrasound transducer array for ultrasound/photoacoustic dual modality imaging. Opt Express 2014;22:26365-74.
46. Thella AK, Rizkalla J, Helmy A, et al. Non-invasive photo acoustic approach for human bone diagnosis. J Orthop 2016; 13:394-400.
47. Lashkari B, Mandelis A. Coregistered photoacoustic and ultrasonic signatures of early bone density variations. J Biomed Opt 2014;19:36015.
48. Feng T, Perosky JE, Kozloff KM, et al. Characterization of bone microstructure using photoacoustic spectrum analysis. Opt Express 2015;23:25217-24.
49. He W, Zhu Y, Feng T, et al. Comparison study on the feasibility of photoacoustic power spectrum analysis in osteoporosis detection. Proceedings of SPIE 10064, Photons Plus Ultrasound: Imaging and Sensing 2017, 100645H; 2017 March

3; San Francisco (CA), USA. https://doi.org/10.1117/12.2250677.
50. Shubert J, Lediju Bell MA. Photoacoustic imaging of a human vertebra: implications for guiding spinal fusion surgeries. Phys Med Biol 2018;63:144001.
51. Zackrisson S, van de Ven SM, Gambhir SS. Light in and sound out: emerging translational strategies for photoacoustic imaging. Cancer Res 2014;74:979-1004.
52. Yao J, Wang L, Yang JM, et al. High-speed label-free functional photoacoustic microscopy of mouse brain in action. Nat Methods 2015;12:407-10.
53. Wang L, Maslov K, Wang LV. Single-cell label-free photoacoustic flowoxigraphy in vivo. Proc Natl Acad Sci U S A 2013;110:5759-64.
54. Jathoul AP, Laufer J, Ogunlade O, et al. Deep in vivo photoacoustic imaging of mammalian tissues using a tyrosinase-based genetic reporter. Nat Photonics 2015;9:239-46.